RAL-TR-2004-028

A PROTOTYPE 2-D GMSD BASED IMAGING DETECTOR FOR NEUTRONS

J.E.Bateman, G.E.Derbyshire, D.M.Duxbury, A.S.Marsh, N.J.Rhodes, E.M.Schooneveld, E.J.Spill and R.Stephenson

Rutherford Appleton Laboratory, Chilton, Didcot, Oxon, OX11 0QX, U.K.

19th November 2004

Abstract

The development and testing of a 2-D prototype imaging neutron detector based on a Gas Microstrip Detector (GMSD) is reported using a gas mixture of 2.5bar ^3He and 2.5bar CF_4. The second spatial co-ordinate is obtained by utilising a plane of wires (orthogonal to the strips) as pick up electrodes. The detector is operated with the wire plane at such a potential so as not to induce any gain around the wires. This means that the high tolerances normally associated with wire planes in Multi-Wire Proportional Counters are not mandatory. The detector comprises of 48 individually instrumented channels in both X (GMSD strips) and Y (transverse wire plane). A specially designed encoding module has been constructed which feeds digital addresses for each event to the ISIS data taking electronics system (DAE). An intrinsic detector resolution of ~1mm FWHM has been measured for both dimensions (in experimental exposures on the ROTAX beam line at ISIS) which is degraded slightly by the digital resolution for the overall system. This readout method is shown to be very tolerant of a poor signal to noise ratio in the readout channels (unlike traditional analogue wire chamber readout systems) and permits the operation of the GMSD at low avalanche gains (~10) which helps to maximise the rate and lifetime performance of the detector as well as permitting data capture rates in the MHz range. The event timing resolution is comfortably sub microsecond and is therefore suitable for applications on spallation neutron sources.

1. Introduction

Gas based detectors of various types are routinely used in the construction of neutron diffractometers [1,2]. For single crystal studies with pulsed neutron sources, such as ISIS, it is desirable to have a detector capable of covering a large area (of order 0.5m^2), whilst having a spatial resolution (in both dimensions) of the order of 1mm with high counting rate capability and microsecond timing resolution. Previous development work has been done with a GMSD based detector as a 1-D device [3,4] and this report details the further development of this detector into a 2-D imaging device.

Key science areas within the UK demand large neutron sensitive detectors with two-dimensional (2-D) readout. These include single crystal (SX) and reflectometry instruments need 200mm x 200mm 2-D detectors to operate on the proposed ISIS target station 2 [5].

We report the successful testing of a small prototype two dimensional gas micro-strip detector of dimensions ~50×50mm capable of MHz readout rates. Various approaches to 2-D readout of GMSDs have been developed [6-8]. We have followed the approach of Budtz-Jorgensen in using a wire plane close to the plate surface to pick up the second dimension [9]. Combining this approach with a channel by channel readout method permits operation with a low detector gain leading to reliable long term operation at high data rates and acceptable spatial resolution. The performance of the detector was measured in tests on the ROTAX beam line of the ISIS facility at the Rutherford Appleton Laboratory.

2. The 2-D GMSD Detector

2.1 Fast 2-D Readout of GMSDs

A complete description of the fast readout of two dimensional GMSDs is given in [10]. The purpose of the prototype detector described in this report is to explore the possibility of generalising the channel-by-channel readout method to achieve full 2-D imaging capability. While the need to correlate the X (anode) signals with the Y (orthogonal wire plane) signals forces the readout to be global (and therefore more rate-limiting than the 1-D case), the occupancy time (i.e. the intrinsic length of the x-ray pulse of ≈200ns) is applied to only one discriminator circuit at a time so that the correlating and coding electronics can, in principle, perform considerably faster than a traditional analogue readout (at MHz rates). In order to achieve pick-up of the GMSD induction pulse in the direction orthogonal to the anodes (Y), a wire plane of 1mm pitch was set at close to the active plate surface at a distance of less than one anode pitch.

2.2 Detailed design

Figure 1 shows a schematic cross-section of the prototype 2-D detector. The S8900 glass plate is glued to a printed circuit board, and the wire plane for the second co-ordinate is mounted from four spacers at the glass edges some 250μm away from the plate surface. A thin aluminium drift plane (5μm) is mounted 6.1mm from the glass surface. The detector is a legacy from a particle physics project [11] having an anode width of 10µm, a cathode width of 90µm and a pitch of 300µm. The wire plane is constructed from gold plated tungsten wires of 100µm diameter, with 48 wires on a pitch of 1mm. The anodes of the glass plate are grouped together in fours in order to match the wire plane pitch, which gives us a pixel size in the X dimension of 1.2mm. 48 groups of anodes are used which gives us an active area of 57.6mm in X by 48mm in Y. The cathodes of the GMSD and the drift plane are held at a negative potential with the anodes fixed at ground. The wire plane is held close to the equipotential voltage at that locus between drift and plate, therefore ensuring that there is no gain coming from the wire plane. This has the advantage that the wire plane can then be made without the high tolerances normally associated with wire based detectors. The structure of figure 1 is then held in a gas tight enclosure with a thinned aluminium window above the drift electrode to permit entry of the neutrons. Gas ports and electrical sockets are provided for interface to the readout system. For the present tests a gas filling of 2.5bar ^3He + 2.5bar CF_4 was used.

2.3 Operating Characteristics

With operating conditions V_c (cathode) = -800V, V_w (wire plane) = -1kV and V_d (drift electrode) = -4kV, the thermal neutrons from an Am:Be source produce the pulse height spectrum shown in figure 2, when two adjacent channels are summed together and connected to a main amplifier/pulse height analyser chain. The peak in the pulse height spectrum corresponding to the Q of the neutron-induced reaction with the ^3He atom (765keV), can be used to estimate the gas gain of the counter and is used to produce the gain curve seen in figure 3. Also shown in figure 3 is the gain curve produced from the wire plane signal. This shows that on average ~15% of the charge produced on the anodes is induced on the wire plane. As described elsewhere [10] this signal level necessitates the use of an extra amplification stage for the wire plane signal in order to drive the readout electronics.

2.4 Electronic readout

The 48 channels in X and Y are individually instrumented with preamplifier, post amplifiers and discriminators as shown schematically in figure 4. The preamplifiers used are 16 channels fast current amplifiers which have been developed elsewhere [11]. The shaping amplifier was specifically designed to plug into the preamp and is described in [12]. Figure 5 shows typical pulses for both X and Y from the preamplifier and shaping amplifier respectively under neutron irradiation. NIM based Lecroy 612 post amplifiers increase the signal size further before the signals are passed to NE 4684 NIM based discriminators. From here the digital signal is then passed to a combining and encoding module, which is described in detail in [10]. This module determines the validity of the events, addresses the events, combines the data and sends it to the ISIS data taking electronics (DAE), which is described elsewhere [13]. The module takes its master trigger from the anode signal and determines if it is a valid event. This is done using an EPROM, which is programmed to accept either single or double (adjacent) channel hits. The EPROM then looks for events on the other 47 channels to veto out any ghost hits. The event is then addressed as a six bit word (dual adjacent hits are assigned to the least significant bit). This is repeated for Y, and the module then combines the two readout channels by forming a coincidence between the synchronised X and Y pulses. The neutron event address is then sent to the DAE. The data capture efficiency has been measured to be greater than 90%.

3. Imaging performance

The detector was installed on the ROTAX beam line of the ISIS spallation neutron source, which is described in [14], which produces 10^7 neutrons per cm^2. The installation is shown in the photograph in figure 6. Figure 7 shows the data obtained, when a mask made from cadmium was placed on the front window of the chamber and illuminated with the direct ROTAX neutron beam. The lettering on the mask is between 3 and 3.5mm wide and is 18mm high which is reflected in the image. The image integrates all neutron flight times (wavelengths).

In order to measure the intrinsic spatial resolution (unlimited by the digital readout) of the detector, a 0.5mm collimated slit beam of neutrons was set up using two B_4C slabs and was scanned across three adjacent pixels in X and three adjacent wires in Y. The X distribution, shown in figure 8, was obtained by summing in Y to produce an X histogram for each scan position. Each distribution was normalised to its centroid and all the distributions summed. This result illustrates the intrinsic detector resolution with a statistically enhanced digital resolution. The procedure was repeated for Y and is shown in figure 9. Gaussian fits to these figures yields a sigma (standard deviation) of 0.454 channels for X and 0.466 channels for Y. This gives us a FWHM resolution of 1.29mm for X and 1.1mm for Y. The practical readout spatial resolution of the detector is of course convolved with the digital resolution of the readout system $W/\sqrt{12}$, where W is the readout pitch, leading to FWHM values of 1.53mm and 1.29mm for X and Y respectively.

The 0.5mm collimated slit beam was then scanned across the entire length of the detector, in both dimensions, in 1mm steps. Figure 10 shows how the measured position and sigma vary across the detector length through the profile along y=25. Figure 11 shows this variation for the Y data along x=25. As can be seen in figure 10, channel x=4 of the detector was not working correctly, which affects the neighbouring channels. This turned out to be a loose connection on the detector.

The rate performance of the system has been measured by using a range of perspex attenuating/scattering sheets, which show that the system will count up to 2×10^5 neutrons per second, see figure 12. The ISIS DAE electronics is only capable of handling time averaged rates of up to 1MHz, although a new version is being made which will double this performance. The system delivers a dead time of ~1μs.

The neutron efficiency of the detector, at 1Å, has been measured to be ~10%. This agrees well with that predicted from Monte Carlo simulation of this detector geometry and ^3He gas pressure [15].

It is important that the detector has a low gamma sensitivity, as the proton-target interaction on the ISIS source produces a large gamma flash. This has been measured with a ^{60}Co source to be of the order of 4×10^{-6}, which is more than acceptable.

The uniformity of the detector response has been measured with X-rays [10] and is found to be 3.2% in the X direction and 6.2% in the Y direction.

4. Timing Performance

The time resolution of the detector is determined by two main effects: the flight time of the neutrons in the 6.1mm deep conversion space and the variation in the drift time of the neutron-induced electron clouds to the GMSD plate.

4.1 Flight time variation

On the ROTAX beam line the detector has a flight path (L) of 14.58m. The detector has a depth of 6.1mm giving $\sigma_L = 1.76$mm ($6.1/\sqrt{12}$) with $\sigma_L/L = 1.21\times10^{-4}$. This gives a timing error proportional to the flight time (wavelength) which is, for example, 0.45μs at 1Å (t= 3757μs).

4.2 Drift time variation

The drift velocity of electrons in the current gas mixture at a drift field of 656V cm^{-1} is approximately 1.2cm/μs [16]. The 6.1mm drift space thus introduces a variation in the drift time of $\sigma_t = 0.61/(1.2\times\sqrt{12}) = 0.15$μs. This variation will be further increased by a few tens of percent by the variation in rise time introduced by the random orientation of the combined track length of the proton and triton (8.3mm). The exact magnitude of the effect depends on the type of pulse discriminator used. Thus over the region of the time of flight (TOF) spectrum of general interest, the neutron flight time variation is the chief source of timing errors.

Figure 13 shows the TOF diffraction spectrum measured by the detector from an Fe sample. The data is summed over the width of a single pixel, column 17, to restrict the range of scattering angle. A Gaussian fit to the diffraction peak at ≈10600μs has a standard deviation of 48μs. As will be shown below, this apparent time resolution is mostly wavelength spread due to the variation in scattering angle arising from the 12mm sample depth. At t=10600μs the RMS flight time error due to the detector is 1.3μs.

5. Application of the Detector to Powder Diffraction

As an application of the detector which would show some of its capabilities, a diffraction experiment was set up using a 12mm×12mm rod of Fe as the sample. The detector was set up at approximately 90 degrees to the beam direction, 57cm from the sample so that the Debye-Scherer (D-S) rings would form vertical lines on the detector.

The TOF curves were extracted for pixels summed up each column (X). Figure 13 shows the TOF curve for the 17th pixel column. The strongest line (at t≈10600μs) is chosen for analysis. As shown, the peak fits well to a Gaussian with a SD of 48.11μs. The Bragg condition for the first order:

$$\lambda = 2d\sin\varphi/2 \qquad (1)$$

relates the centroid of the TOF peak (i.e. wavelength λ) to the angle of the D-S line on the detector (i.e. data column, φ) and the lattice constant d. Figure 14 shows a plot of the fitted TOF peak centroid for each pixel column against the pixel number, each pixel represents 2.12mr in angle. This gives an experimental value for the lattice constant d, of 1.93Å which agrees well with the theoretical value of 2.02Å.

The width of the pixel column does not define the error in the angular measurement. This is affected by such things as the finite sample size and timing errors. In order to see this effect detector images were generated in time windows which scanned across the region of the strong peak in the TOF spectrum. Starting at T=10293µs, images were generated in 7 successive windows of width ~64µs. The D-S ring could now be seen crossing the detector in figure 15. It is obvious to the eye that the peaks are not Gaussian, and the figure shows that a log-normal distribution (with a background term) fits much better (The peak of the log-normal distribution is not c but $c \times \exp(-b^2)$, and the equivalent of sigma is bc). The points on the graph show the experimental data and the curves are the log-normal fits to these points. Figure 16 shows the D-S line for time slice 10654µs. The data fits acceptably to a log-normal curve and the position (angle) can be measured with an accuracy of σ= 0.138pixels i.e. 0.29mr. The SD of the D-S rings is 4.795pixels i.e. 5.75mm (10.17mr). The contributions of the various errors to the width of the D-S line can be estimated from equation (1), which for small angles about φ=90° approximates to:

$$\Delta\lambda = d\,\Delta\varphi/\sqrt{2} \qquad (2)$$

The relationship t= 3758.2λ inter-converts TOF (µs) and wavelength (A). Using these relations, and to a first order approximation, it is found that the TOF window of 64µs gives an RMS error of 3.6mr in angle, the sample depth (12mm) gives 11.9mr and the detector flight time variation gives 0.25mr. Combining these in quadrature gives a final SD of 12.4mr for a D-S line. This is in reasonable agreement with the value of 10.2mr observed.

6. Discussion

The results presented above from the prototype 2-D GMSD show that a high rate (>MHz) 2-D neutron detector design with millimetre spatial resolution can be based on the principles described. The target design would aim at an active area of 200mm x 200mm with a plate anode pitch of 1mm and a Y wire plane of the same pitch with a neutron detection efficiency of >50% at 1Å. Further work is required to define the upper rate limit of the encoding system and the connection to an adequately speedy data capture system.

Funding has been secured, via the centre for instrumentation, to build a 200 by 200mm version of this detector. This detector will be specifically designed as an x-ray detector with the gas filling at atmospheric pressure, but a similar detector mounted in an atmosphere of pressurised ^{3}He would be suitable for neutron imaging.

References

1. S. Katano, Y Ishii, Y. Mori, H. R. Child, J. A. Fernandez Baca, Physica B 241-243 (1997) 198

2. P. Convert, T. Hansen, A. Oed, J. Torregrossa, Physica B 241-243 (1997) 195

3. J. E. Bateman, N. J. Rhodes, R. Stephenson, RAL-TR-1997-021

4. J. E. Bateman, N. J. Rhodes, R. Stephenson, Nucl. Instr. and Method A 477 (2002) 365

5. A. Taylor, Physica B 276-278 (2000) 36-37

6. F. Angelini, R. Bellazini, L. Bosisio, A. Brez, M. M. Massai, A. Perret, G. Spandre and M. R. Torquati, Nucl. Instr. and Method A 323 (1992) 229

7. H. Takahashi, K. Yokoi, K. Yano, D. Fukuda, M. Nakazawa and K. Hasegawa, Nucl. Instr. and Method A 471 (2001) 120

8. S. F. Biagi, J. Bordas, D. Duxbury, E. Gabathuler and T. Jones, Nucl. Instr. and Method A 336 (1995) 76

9. C. Budtz-Jorgensen, Rev. Sci. Instrum. 63 (1) (1992) 648

10. J. E. Bateman, G. E. Derbyshire, D. M. Duxbury, A. S. Marsh, N. J. Rhodes, E. M. Schooneveld, E. J. Spill, R. Stephenson RAL-TR-2004-027

11. J. E. Bateman, J. F. Connolly, R. Stephenson, M. Edwards and J. C. Thompson, Nucl. Instr. and Method A 348 (1994) 372

12. A. D. Smith, J. E. Bateman, G. E. Derbyshire, D. M. Duxbury, J. Lipp, E. J. Spill and R. Stephenson, Nucl. Instr. and Method A 467-468 (2001) 1136

13. M. W. Johnson, S. P. Quinton RAL-NDRP-8504

14. W. Schäfer, E. Jansen, R. Skowronek, G. Will, W. Kockelmann, W. Schmidt, H. Tietze-Jaensch, Nucl. Instr. and Method A 364 (1995) 179

15. J.E. Bateman, N. J.Rhodes, R. Stephenson, RAL-TR-1998-024

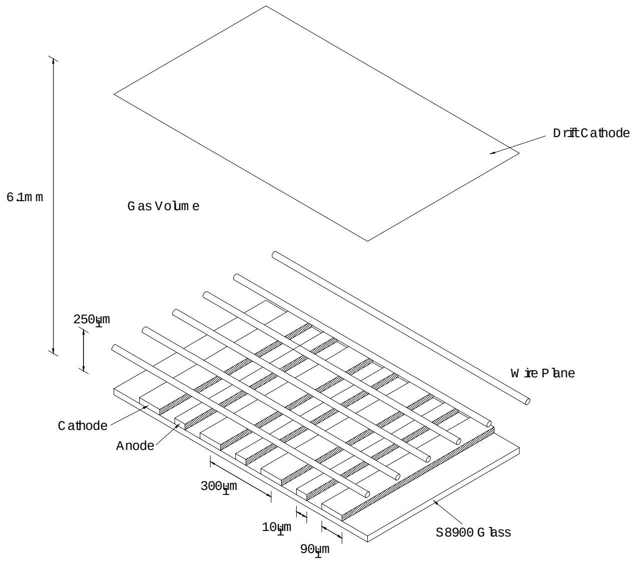

Figure 1: Schematic diagram of the detector geometry

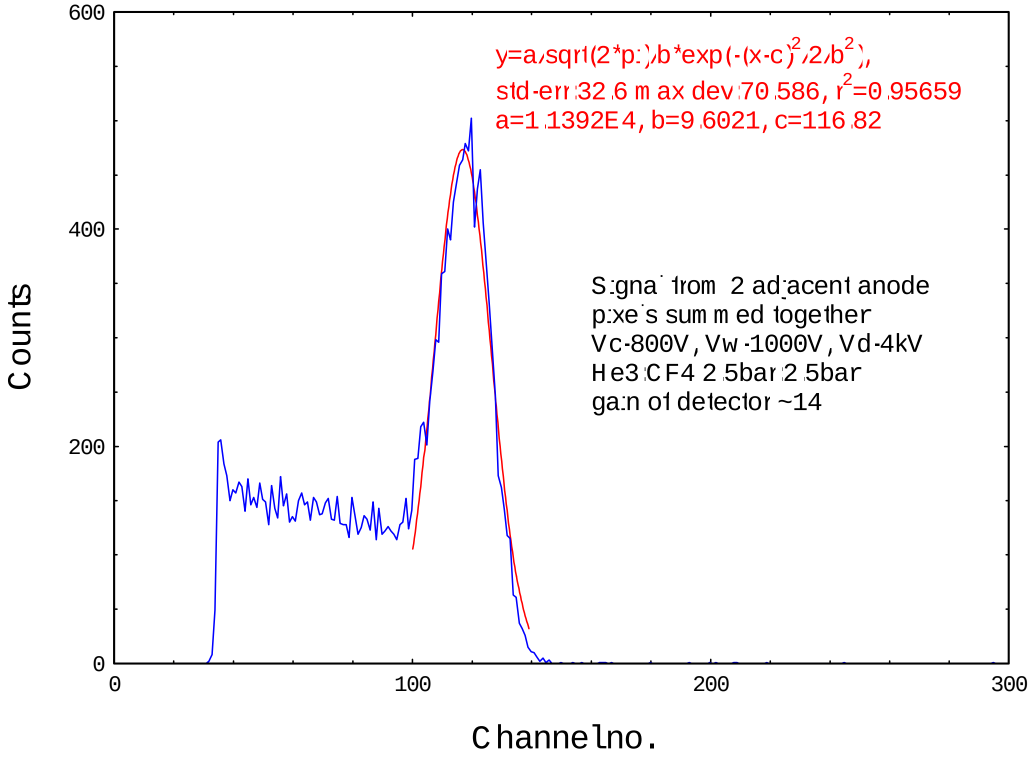

Figure 2: Neutron-induced pulse height spectrum taken from the sum of two adjacent channels

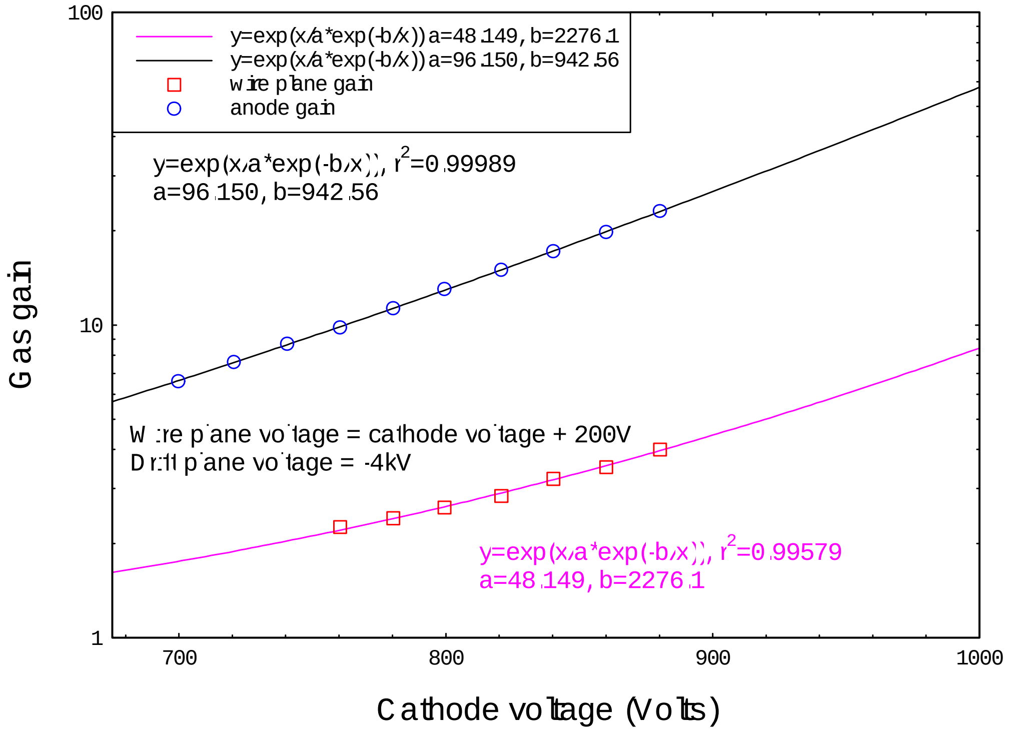

Figure 3: Gain variation of the GMSD anodes and wire plane as a function of voltage under neutron irradiation

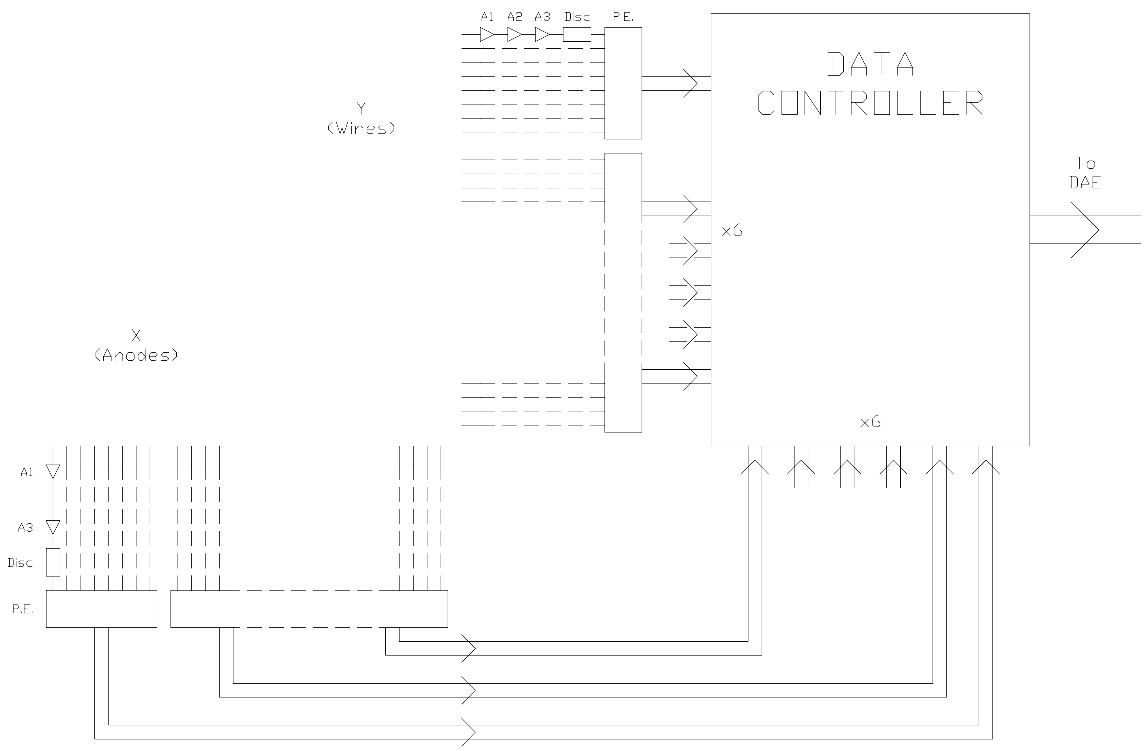

Figure 4: Schematic diagram of the electronic readout. Where A1 is the 16 channel preamplifier; A2 is the shaping amplifier; A3 is the NIM postamplifier; Disc is the NIM discriminator and PE is the primary encoder

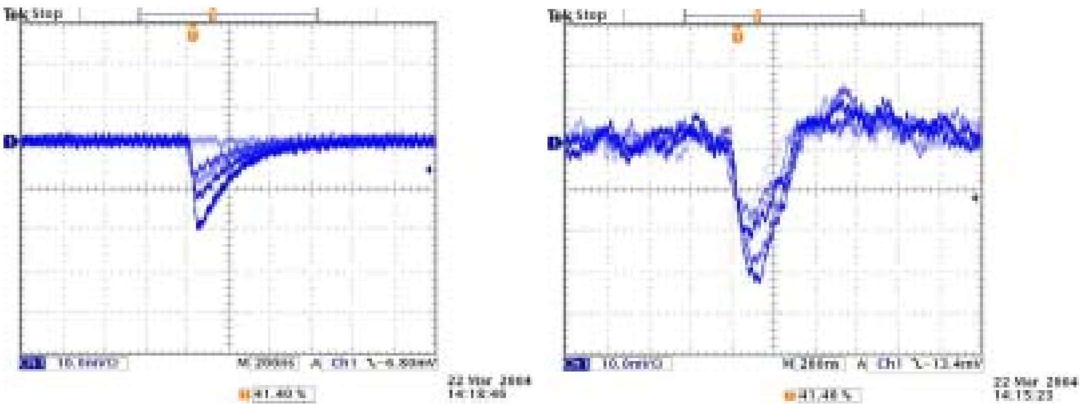

Figure 5: Typical pulses from the GMSD preamp (left) and wire plane preamp/shaper (right) for neutrons.

Figure 6: Photograph of the detector on the ROTAX beam line at 90^{o} to the sample position

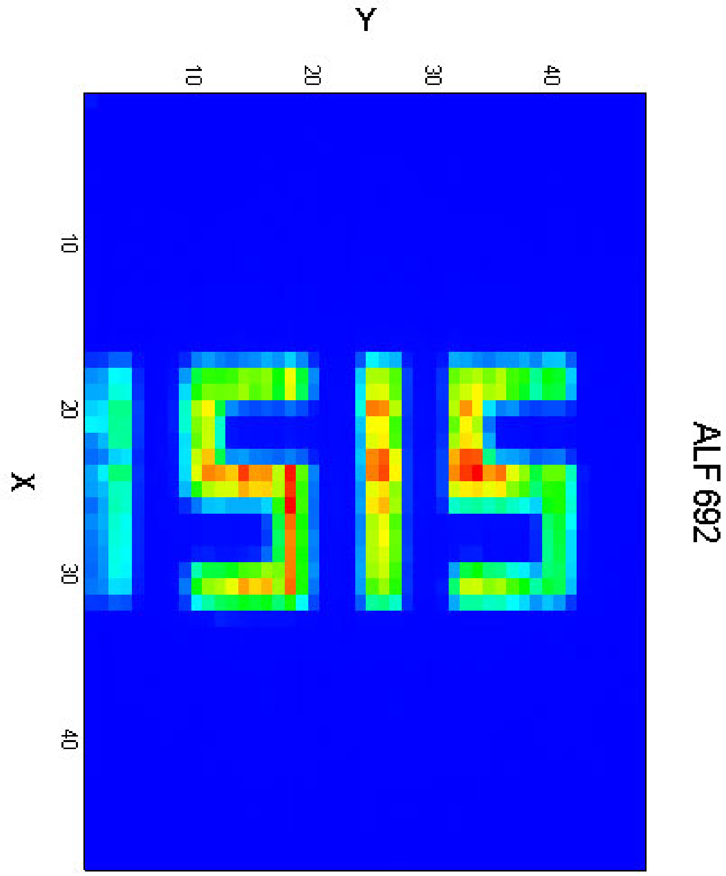

Figure 7: Image of cadmium 'ISIS' mask taken on ROTAX

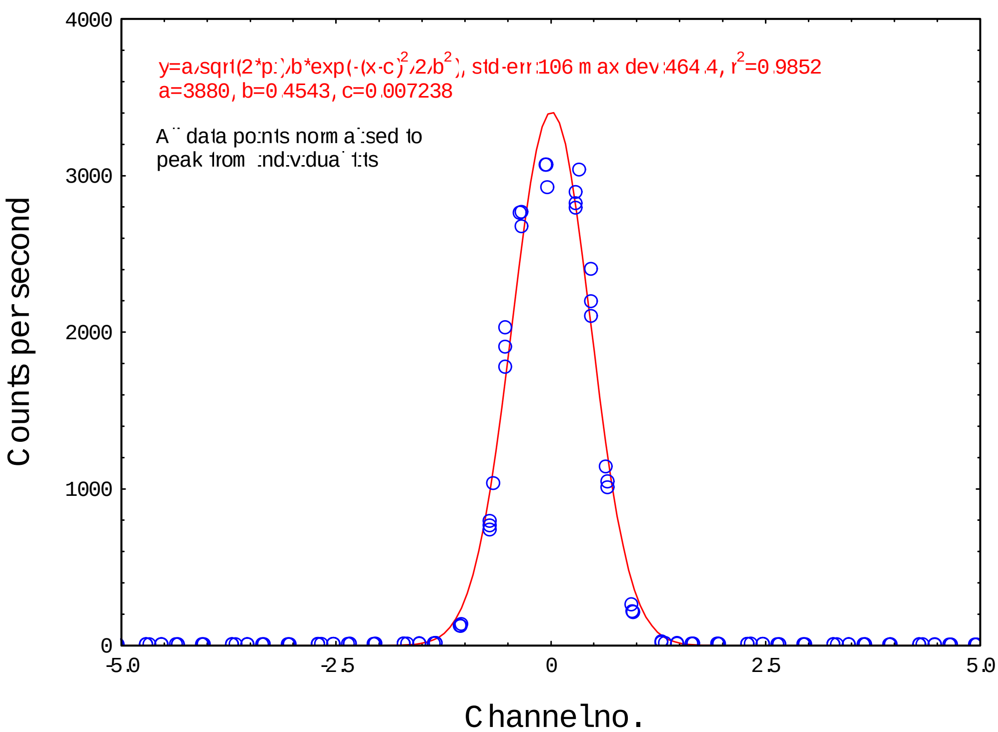

Figure 8: Intrinsic detector spatial resolution using interpolated readouts for X

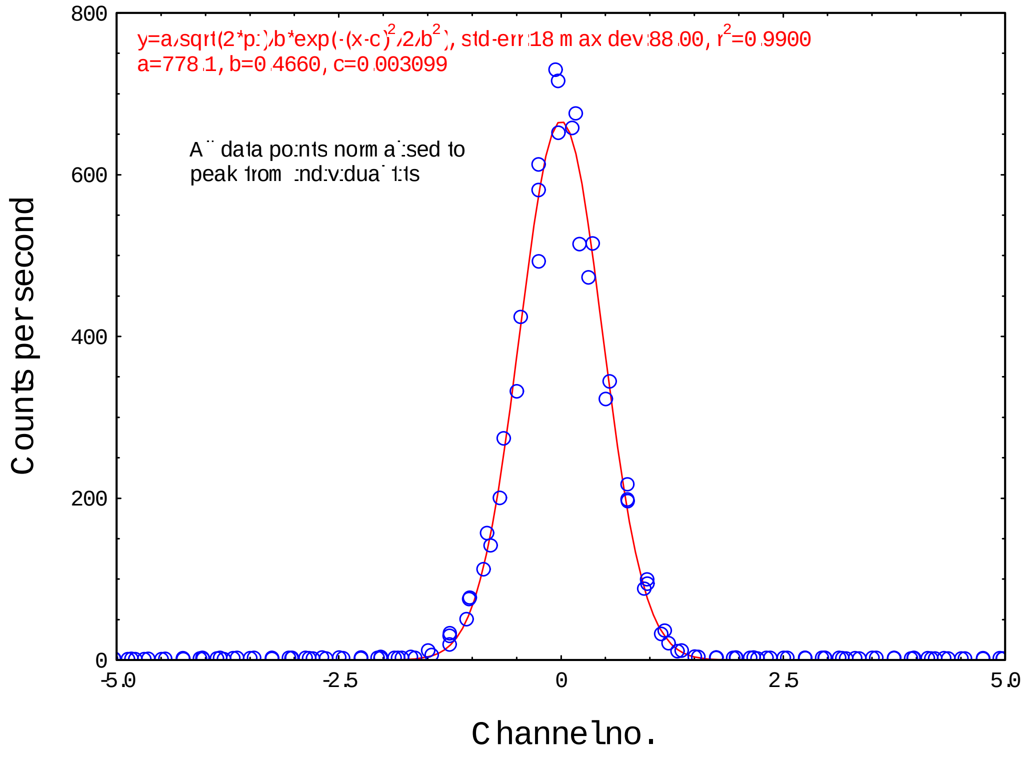

Figure 9: Intrinsic detector spatial resolution using interpolated readouts for Y

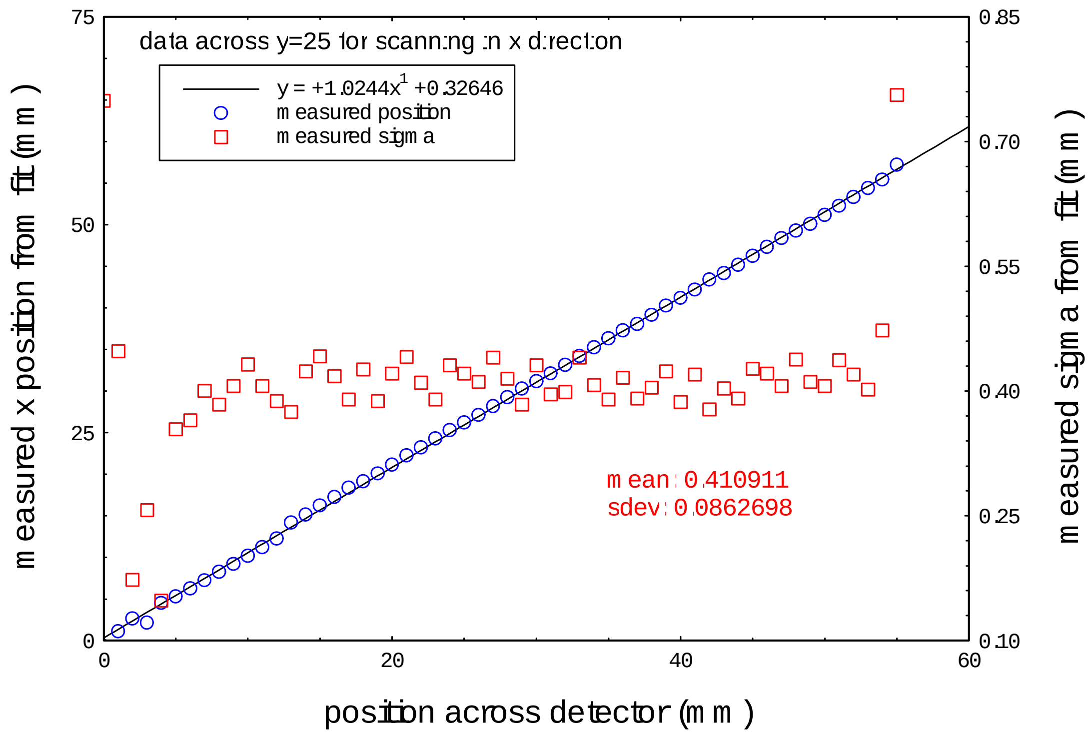

Figure 10: profile along y=25 for 0.5mm collimated beam scanned in X direction

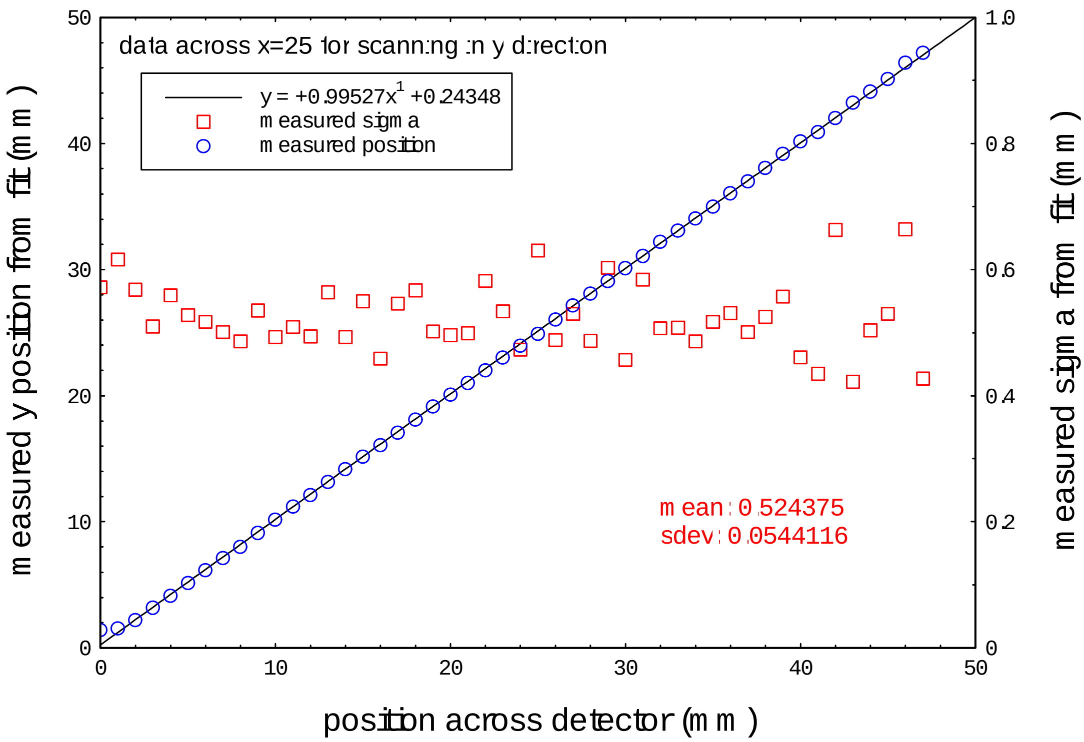

Figure 11: profile along x=25 for 0.5mm collimated beam scanned in Y direction

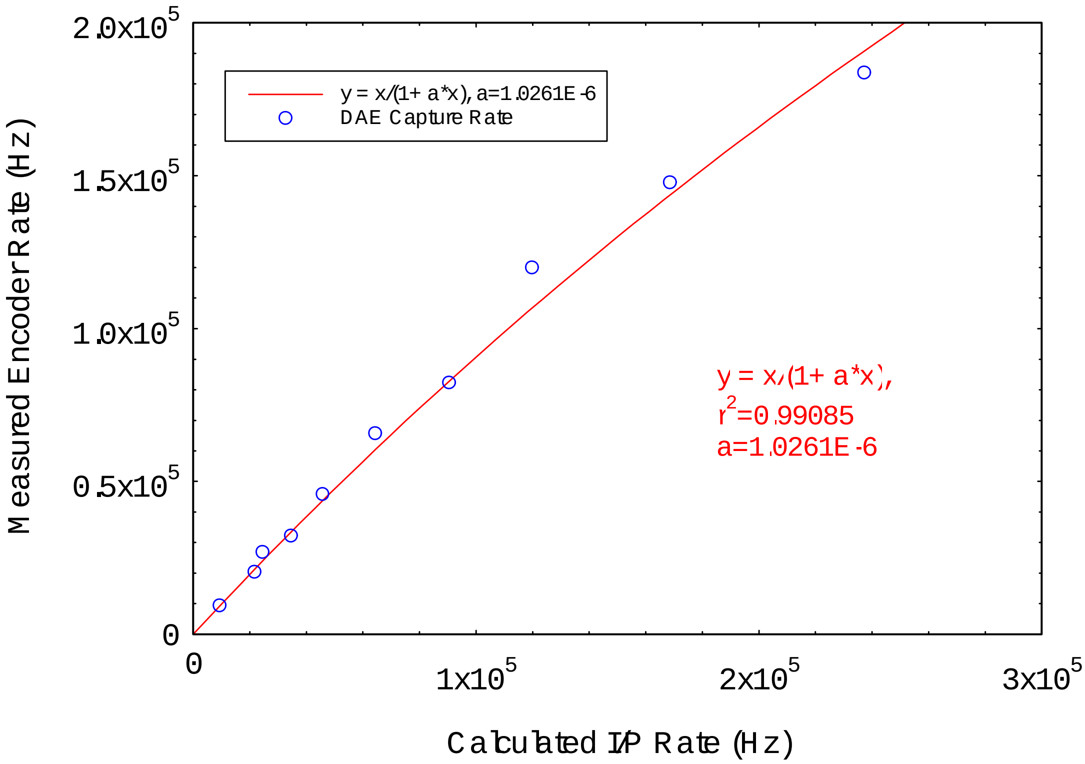

Figure 12: Dead time curve of the system on ROTAX

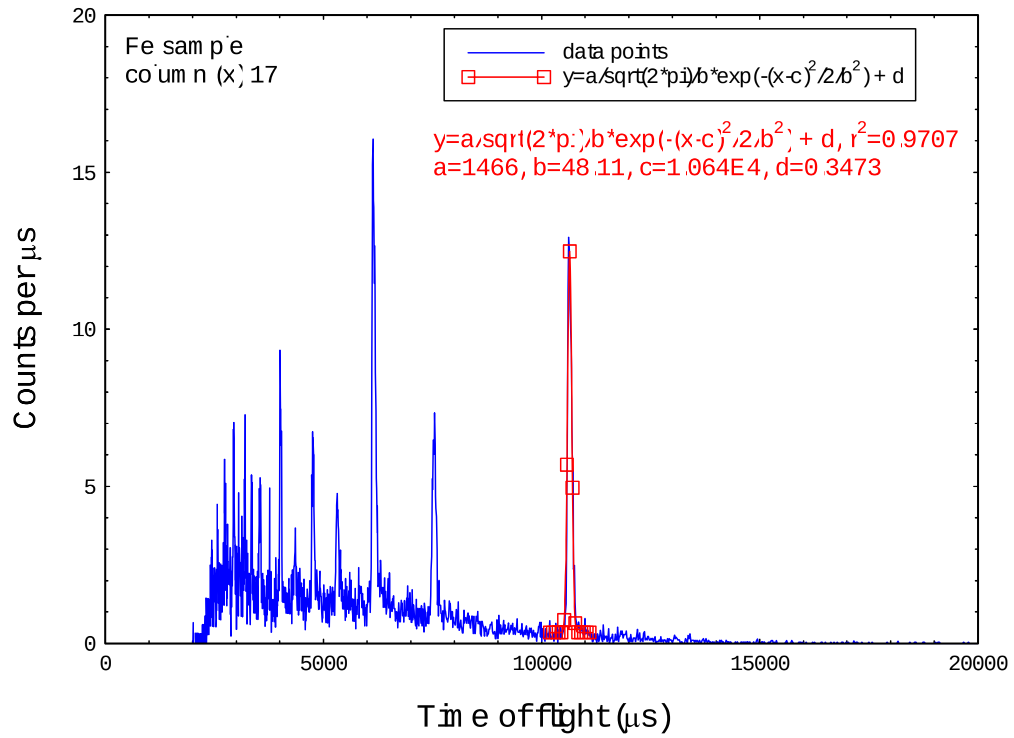

Figure 13: Time of flight spectrum for Fe sample on ROTAX as measured with the 2-D GMSD detector

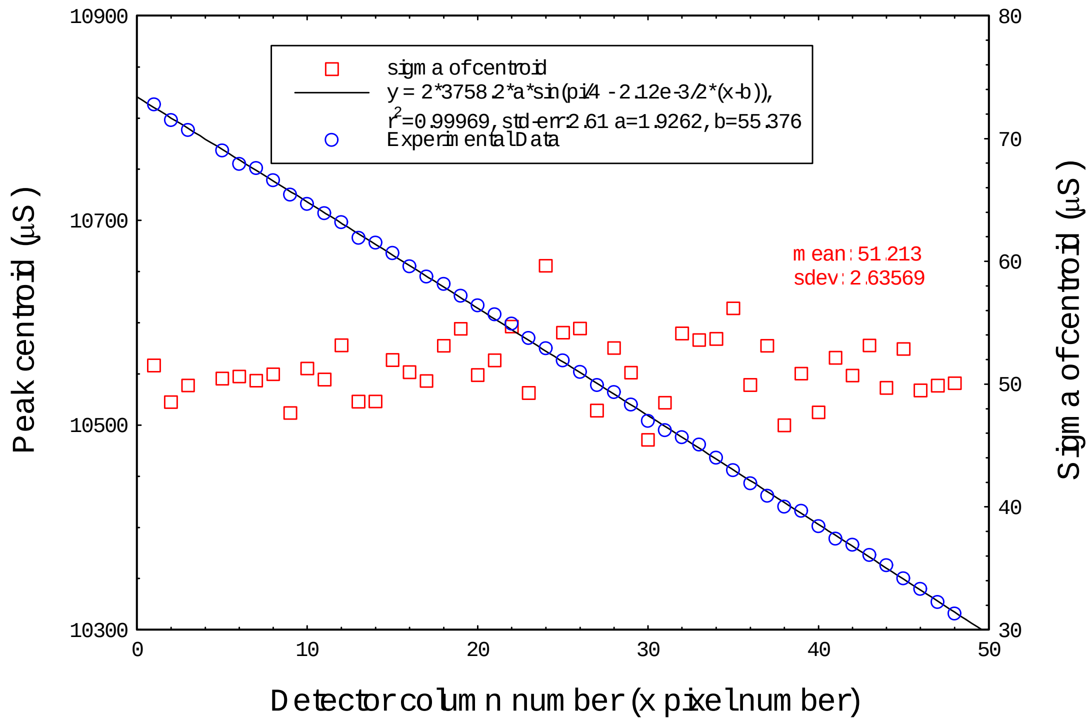

Figure 14: TOF peak centroid and sigma for each pixel column vs the column number

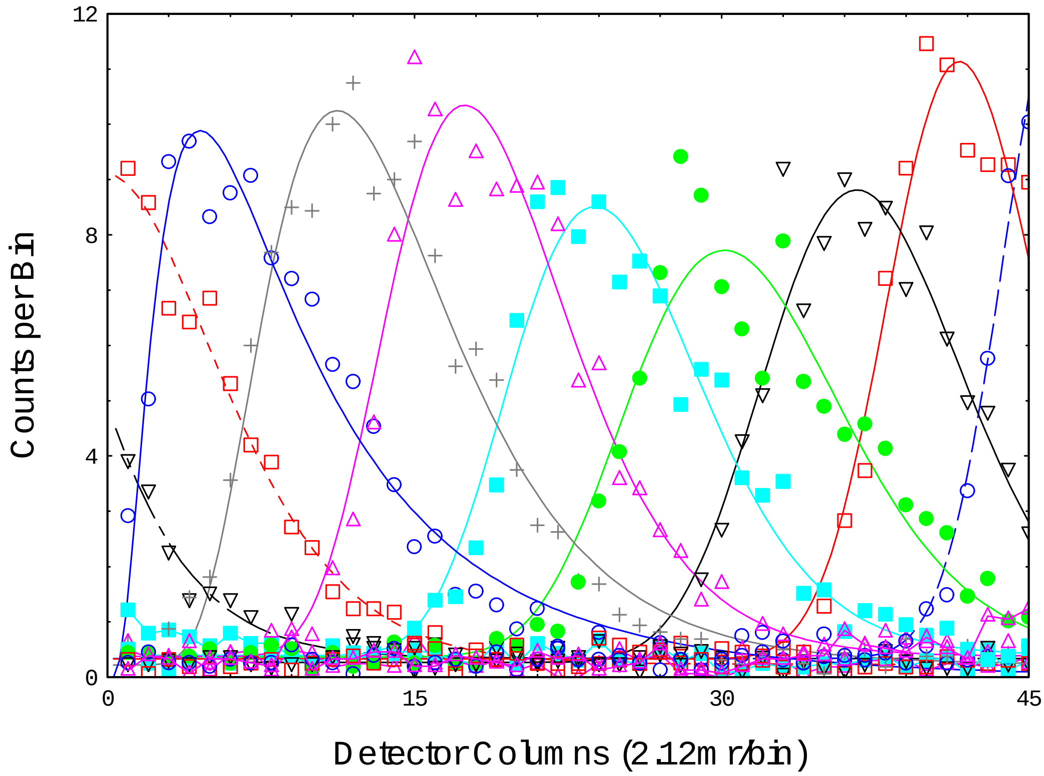

Figure 15: D-S lines crossing the detector in 64μs intervals. The markers show the experimental data, and the curves show log-normal fits to these data points.

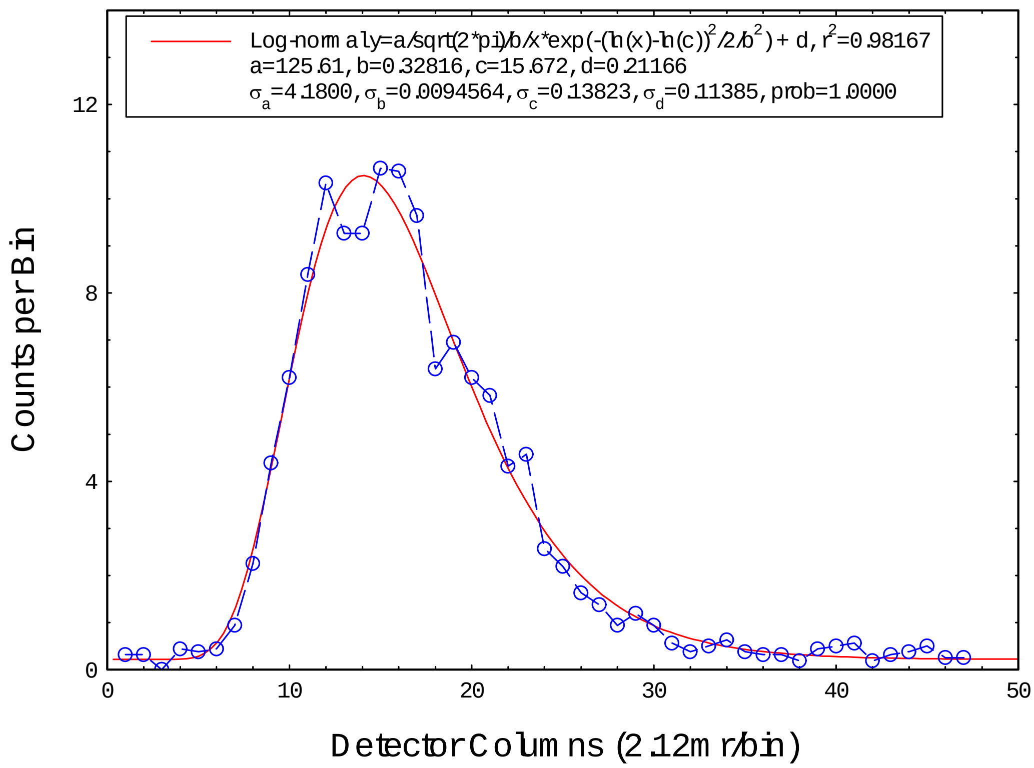

Figure 16: D-S line at t=10654μs